The Nucleus ***61***, *No. 2 (2024) 101-107*

www.thenucleuspak.org.pk

The Nucleus

ISSN 0029-5698 (Print)
ISSN 2306-6539 (Online)

Comparative Analysis of Torsional and Tensile Load Performance of Interference Screws Made of Titanium, PEEK, and PLLA: A Numerical Study

Muzalil Hussain[1], Shahzad Maqsood Khan[1], Muhammad Shafiq[1], Naseem Abbas[2], Aqeel Abbas[3*]

[1]*Institute of Polymer & Textile Engineering, University of the Punjab, Pakistan*

[2]*Department of Mechanical Engineering, Sejong University, Seoul 05006, Korea*

[3]*Department of Mechanical Engineering, NFC Institute of Engg. & Fertilizer Research Faisalabad, Pakistan*

ABSTRACT

Interference screws are widely used for soft tissue-to-bone or bone-to-bone graft fixation, with the choice of material being crucial for successful outcomes. This study compares the performance of interference screws made of titanium, polyetheretherketone (PEEK), and poly-L-lactic acid (PLLA) under torsional and tensile loads using a finite element model. The mechanical results showed that the mean value of the moment to failure was 15.06 Nm for titanium, 1.54 Nm for PEEK, and 0.797 Nm for PLLA. The mean load to failure of the interference screw was 6493.13 for titanium, 640.71 for PEEK, and 31.76 Nm for PLLA. The titanium exhibits the highest moment and load to failure under torsional and tensile loads. PLLA exhibits the lowest and PEEK exhibits the intermediate results. PLLA exhibits less deformation under tensile and torsional load, which makes it suitable for load-bearing applications.

Keywords: *Biomaterials, Orthopedic implants, Interference screw, Failure analysis, Biomedical devices*

1. Introduction

The successful reconstruction of the anterior cruciate ligament (ACL) requires a secure fixation of the graft in both the femoral and tibial tunnels, and interference screws play a crucial role in this process [1]. The choice of material for these screws is pivotal, with commonly used options being titanium, polyetheretherketone (PEEK), and poly-L-lactic acid (PLLA) [2-4].

Titanium screws are widely employed for ACL reconstruction due to their strength and stiffness, ensuring a secure graft fixation—a prerequisite for success. However, challenges during insertion can arise due to their higher hardness [5]. PEEK interference screws, an alternative to titanium, offer radiolucency for artifact-free imaging and an elastic modulus similar to bone, potentially reducing stress shielding. Moreover, they do not cause tunnel widening, a concern with titanium screws after hamstring ACL reconstruction [6]. PLLA interference screws, being bioresorbable, can mitigate cyst formation and bone destruction over time, although they may present complications such as pain at the screw site [7].

Advancements in interference screw materials aim to enhance functionality, with current biodegradable options including degradable metal-based materials like Mg-based, Zn-based, and Fe-based alloys, as well as polyester-based degradable polymers or their composites [8-15]. Metallic biodegradable materials, especially Mg-based ones, are gaining attention due to their high bioactivity, precise degradation, and excellent mechanical properties [16, 17]. Mg-based materials offer biocompatibility, biodegradability, and mechanical strength, making them attractive for medical applications. Crucially, unlike permanent implants requiring secondary removal surgery, magnesium-based biodegradable materials gradually dissolve and get metabolized by the body, reducing long-term complications and eliminating the need for additional surgery [18, 19].

Screws made of biodegradable materials are easily degradable in the body, with PLA breaking down into lactic acid and glycolic acid, and PGA [20, 21]. However, the downside of bioresorbable interference screws is that they can lead to bone destruction and cyst formation during the hydrolytic process and may cause complications such as pretibial pseudocyst and pain at the tibial screw site [22, 23]. Combining these PLA isomers alone can affect the degradation time and mechanical strength. Hydroxyapatite (HA) and Beta-tricalcium phosphate (ß-TCP) are widely used as bone void fillers due to their excellent biocompatibility with bone and mineral content that closely resembles natural bone [24-26]. However, like polymers, these materials also have issues with resorbability. HA has a slow resorption rate and can take years, while ß-TCP resorbs quickly and exhibits improved bone formation ability [27-29]. ß-TCP is also combined with HA to improve the bone formation ability [30, 31].

The commercial sector is investing large amounts in the research and development of innovative materials. A variety of materials are in the research and development phase for interference screws. Testing interference screws made of different materials has certain limitations that researchers must be aware of, including variability in material properties, complexity of mechanical testing, and difficulty in establishing clinical relevance. Numerical simulation using commercially available packages can become an important tool for testing interference screws under mechanical testing because they can provide researchers with a fast, cost-effective, and detailed way to evaluate the screws' performance under different conditions and to optimize the properties of materials and their design for improved performance. This research focuses on the testing of interference screws made of different available materials.

*Corresponding author: engr.aqeel14@gmail.com

The objective of this research is to present the method for identifying other suitable innovative materials.

2. Material and Methods

2.1 Geometry

Round head and fully threaded interference screws with different sizes have been introduced by many companies such as Stryker, Zimmer Biomet, Arthrex, etc. All these companies provide approximate similar designs and dimensions of interference screws. The round head design of the Arthrex interference screw (10 × 35) was selected for this research. The screw was modelled using PTC Creo Parametric. The length and major diameter of the screw were 35 mm and 10 mm respectively. The threaded profile was created by sweeping a cut profile on a helical path in such a way that the minor diameter gets smaller at the tip of the screw. A hole of the diameter was created in the screw. The hexagonal socket head of the diameter was made.

2.2 Meshing

ANSYS static structural module was used to create the meshed geometry of the interference screw. Tetrahedral mesh-type geometry is shown in Fig. 1. 150,000 elements were used for the computational analysis.

Fig. 1. Meshed geometry of interference screw

2.3 Boundary conditions

The interference screw was tested under insertion torsional and tensile load. For tensile testing, one end of the screw was fixed and on the other end, a tensile load was applied as shown in Figure 2a. A torque load was used on the same end for producing torque as shown in Figure 2b. First, the interference screw was tested on an 877 N tensile load and 15603 N-mm moment, and the factor of safety was noted in these loading conditions. Then, the load to failure at yielding was predicted by using the values of applied load and factor of safety. Maximum equivalent stress and deformation were predicted against the same values of the factor of safety.

This research focuses on the testing of interference screws made of titanium, PLLA, and PEEK. The properties of materials as input parameters are given in Table 1.

The loads were applied and the finite element model was solved using ANSYS static structural. The maximum stress and displacement were compared to the yield strength and deformation limit of the screw material to determine if the screw is safe under the applied load. Table 2 demonstrates that as mesh density increases, the quality of elements (measured by skewness) improves, and simulation results for maximum equivalent stress and deformation converge. At 100,000 elements, there is reasonable accuracy, but grid independence is achieved at around 150,000 elements, with stable results for deformation (~0.318 mm). Using 508,000 elements further improves skewness quality but provides negligible changes in results. Therefore, 150,000 elements were used for the computational analysis.

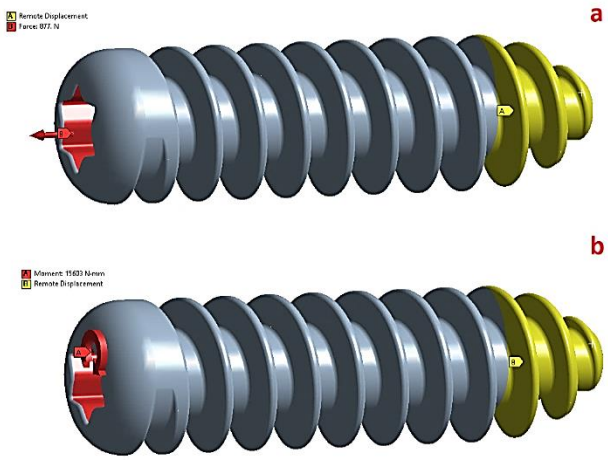

Fig. 2. Interference screw under load (a) tensile load (b) torsional load

Table 1: Material properties as input parameters for numerical simulation in ANSYS.

Property	PLLA	PEEK	Titanium Ti-6Al-4V
Density g/cm^3	1.25	1.31	4.43
Yield strength MPa	60	115	1170
Melting Temperature ^oC	160 - 170	350	1660
Modulus of Elasticity MPa	3500	4100	113800
Ultimate strain	6 %	15%	10 %
Elongation at break	<5%	15 %	10 %
Poison ratio	0.3	0.4	0.342

Table 2: Grid independence test and skewness distribution for numerical simulation in ANSYS.

Mesh Quality (elements)	Skewness distribution (Quality)	Maximum deformation (mm)
100,000	68% (0.0 – 0.25), 25% (0.25 – 0.5), 7% (0.5 – 0.75)	0.2356
125,000	70% (0.0 – 0.25), 26% (0.25 – 0.5), 4% (0.5 – 0.75)	0.3058
150,000	72% (0.0 – 0.25), 27% (0.25 – 0.5), 1% (0.5 – 0.75)	0.3177
500,000	75% (0.0 – 0.25), 24% (0.25 – 0.5), 1% (0.5 – 0.75)	0.3178

2.4 Estimation of equivalent stresses and deformation

Assuming the interference screw has a cylindrical geometry with radius R, length L, and shear modulus G: Maximum equivalent stresses (τ_{max}) can be calculated using Equation 1.

$$\tau_{max} = \frac{TR}{J} \quad (1)$$

Where T is applied torque and J is polar moment of inertia which can be calculated by using equation 2.

$$J = \frac{\pi R^4}{2} \quad (2)$$

Equivalent von-mises stresses (σ_{eq}) were calculated using Equation 3.

$$\sigma_{eq} = \sqrt{\frac{3}{2}\tau_{max}} \quad (3)$$

The shear strain was calculated using equation 4.

$$\gamma = TL\ /GJ \quad (4)$$

The deformation θ was calculated using equation 5.

$$\theta = \frac{TL}{GJ} \quad (5)$$

Assuming the interference screw has a cylindrical geometry with radius R, length L, and Young's modulus E for finding the equivalent stresses and deformation under tensile load. The maximum tensile stress was calculated using Equation 6.

$$\sigma_{max} = \frac{F}{A} \quad (6)$$

Where F is the applied axial load and A is the cross-sectional area ($A = \pi r^2$). Equivalent von-mises stress (σ_{eq}) was calculated using equation 7.

$$\sigma_{eq} = \sqrt{{\sigma_{max}}^2 + 3\tau^2} \quad (7)$$

Where τ is the shear stress due to axial load, which was calculated by equation 8.

$$\tau = \frac{F}{2A} \quad (8)$$

The tensile strain was calculated by $\varepsilon = \frac{\sigma_{max}}{E}$ and axial deformation was calculated by equation 9.

$$\delta = \frac{FL}{AE} \quad (9)$$

Result and Discussion

3.1 Titanium

Stress distribution in the case of titanium interference screw is in the range of 1.7951 to 1170 MPa. The stress distribution in an interference screw under torsional load is primarily caused by the uneven distribution of torque throughout the screw. The torque is applied at one end of the screw, and as it travels along the length of the screw, it encounters varying levels of resistance from the bone and surrounding tissue. This results in areas of high stress where the torque encounters the greatest resistance and areas of lower stress where the resistance is lower. The results are presented in Figure 3a.

The failure of an interference screw to torsional load is typically concentrated at the point where the screw threads meet the bone, making it prone to failure. High stress is also observed near the head during initial torque application. On the other hand, the mid-shaft region of the screw, characterized by its larger diameter, serves as the strongest point, effectively resisting bending and torsional forces. The thread profile, particularly deeper threads, enhances resistance against pull-out forces. This information, visually represented in the figure, highlights the critical importance of comprehending both the weakest and strongest points of an interference screw under torsional load. Such insights are pivotal in designing more reliable and durable screws capable of withstanding the stresses encountered during orthopedic procedures.

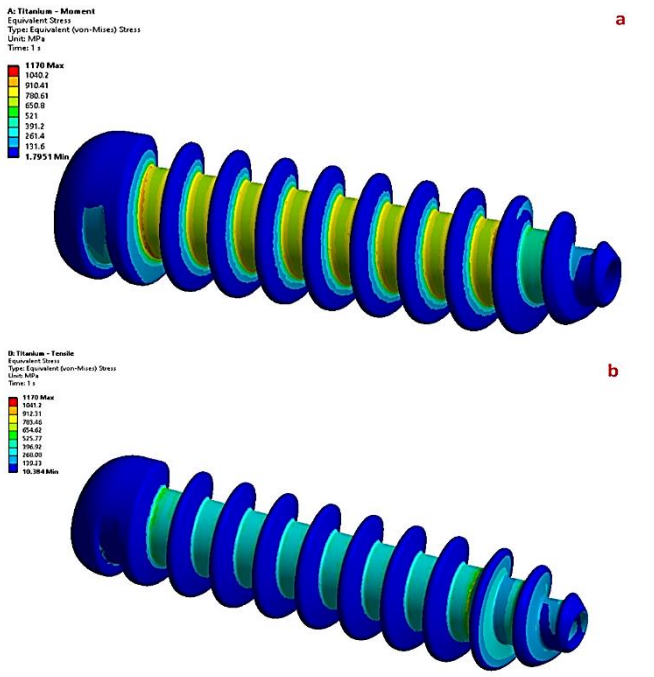

Fig. 1. Stress distribution (a) under torsion load (b) under tensile load

When a tensile load is applied to an interference screw, it is directed to the screw's head while the tail end remains fixed. This setup generates a tension force transmitted along the screw's length, leading to a stress distribution that varies from the head to the tail end. The maximum stress occurs near the head due to force concentration in this region and the reduced cross-sectional area of the screw. As the load progresses along the screw, stress gradually decreases, reaching a minimum near the tail end where the screw is anchored to the bone. The stress distribution under tensile load is presented in Figure 3b. The stress distribution under tensile load mirrors that under torsional load, as varying levels of resistance along the screw's length lead to areas of high stress and lower stress.

Maximum deformation under torsion load acts at the head end due to the application of torsion load at this end. Under tensile load, the screw undergoes an elongation deformation, with the head end being pulled away from the tail end. This elongation creates tensile stresses within the screw, resulting in a strain that is highest near the head and lowest near the tail end. The deformation under tensile load can also lead to failure modes such as screw pull-out or screw breakage. The deformation under torsion load and tensile load is shown in Figure 4a and Figure 4b.

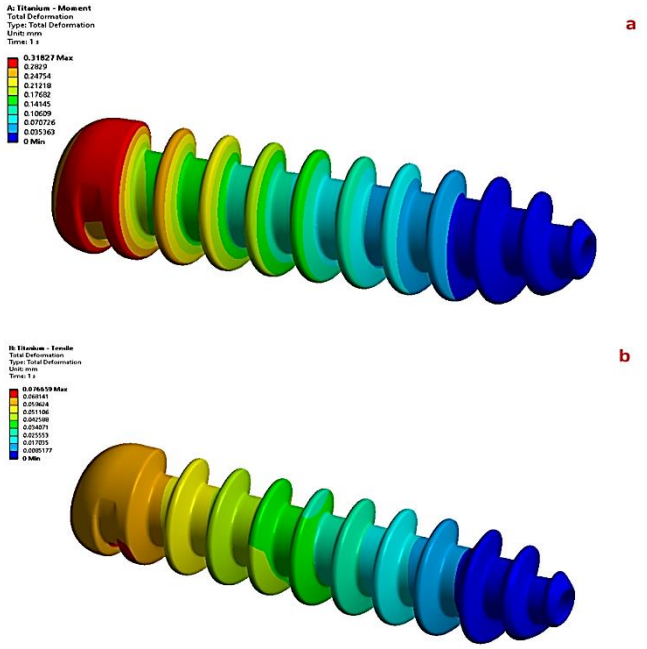

Fig. 4. Deformation under (a) torsion load (b) tensile load

3.2 PEEK

Interference screws made of PLA exhibit 60 MPa maximum equivalent stress. The stress distribution in an interference screw due to the uneven distribution of torque throughout the screw is shown in Figure. The minimum equivalent stress at the interference screw under torsional load occurs near the head and tail at the shortest diameter of the screw as shown in Figure 5a. The maximum stress occurs at the largest diameter of the interference screw. The weakest and strongest points of interference screw under torsional load can be better visualized from the factor of safety distribution under torsional load. The stress distribution of the interference screw under tensile load varies from the head to the tail end as shown in Figure 5b. The maximum stress under tensile load occurs near the head, where the load is initially applied. The minimum stress occurs near the tail end, where the screw is fixed. The maximum stress in the interference screw under tensile load occurs on the fewer portions of a screw as compared to stress distribution under torsional load. The results showed that interference screws under tensile load performed better as compared to torsional load.

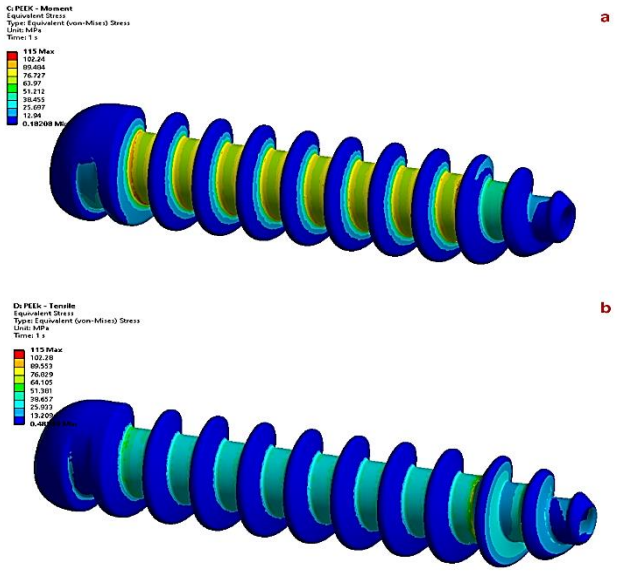

Fig. 5. Equivalent stress distribution under (a) torsional load (b) Tensile load

The maximum deformation under torsional occurs near the head and minimum strain occurs near the tail end due to the shear stresses as a result of twisting motion. The deformation distribution is shown in Figure 6a. The maximum deformation under tensile load occurs near the head and minimum near the tail end due to the uneven distribution of tensile stress within the screw. The deformation under tensile load is significantly less as compared to the deformation under torsional load. The factor of safety distribution clearly showed that the interference screw under tensile load exhibits less failure as compared to the interference screw under tensile load. The results are shown in Figure 6b.

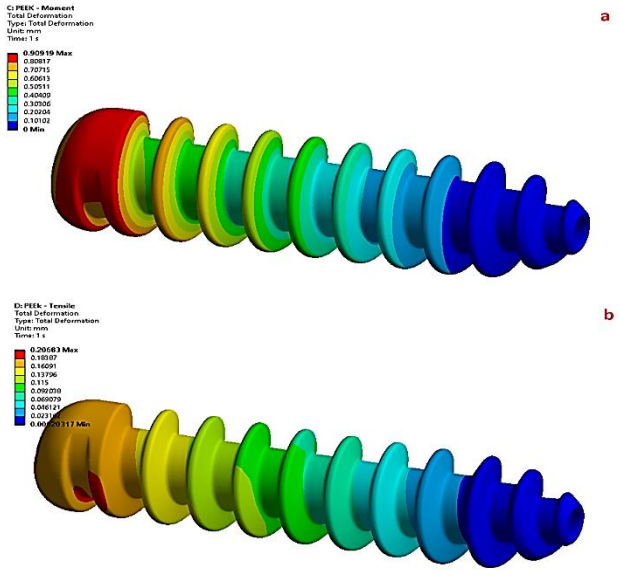

Fig. 6. Deformation under (a) torsional load (b) Tensile load

3.3 PLA

Interference screws made of PLA exhibit 60 MPa maximum equivalent stress. The stress distribution in an interference screw due to the uneven distribution of torque throughout the screw is shown in Figure. The minimum equivalent stress at the interference screw under torsional load occurs near the head and tail at the shortest diameter of the screw Figure 7a. While the maximum stress occurs at the largest diameter of the interference screw. The stress distribution of the interference screw under tensile load varies from the head to the tail end as shown in Figure 7b. The maximum stress under tensile load occurs near the head, where the load is initially applied. The minimum stress occurs near the tail end, where the screw is fixed. The maximum stress in the interference screw under tensile load occurs on the fewer portions of a screw as compared to the stress distribution under the torsional load. The results showed that interference screws under tensile load performed better as compared to torsional load.

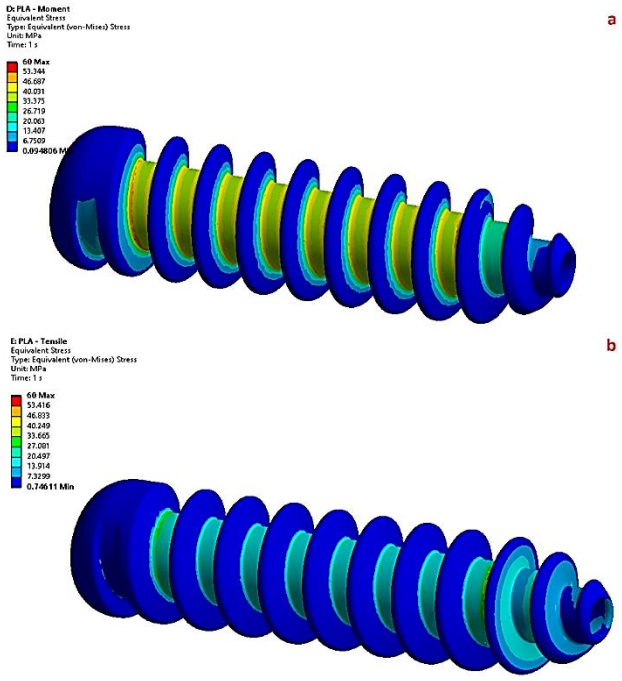

Fig. 7. Equivalent stress distribution under torsional load

The maximum deformation under torsional occurs near the head and the minimum strain occurs near the tail end due to the shear stresses as a result of twisting motion. The deformation distribution is shown in Figure 8a. The maximum deformation under tensile load as shown in Figure 8b occurs near the head and minimum near the tail end due to the uneven distribution of tensile stress within the screw. The deformation under tensile load is significantly less as compared to the deformation under torsional load. The factor of safety distribution clearly showed that the interference screw under tensile load exhibit less failure as compared to the interference screw under tensile load.

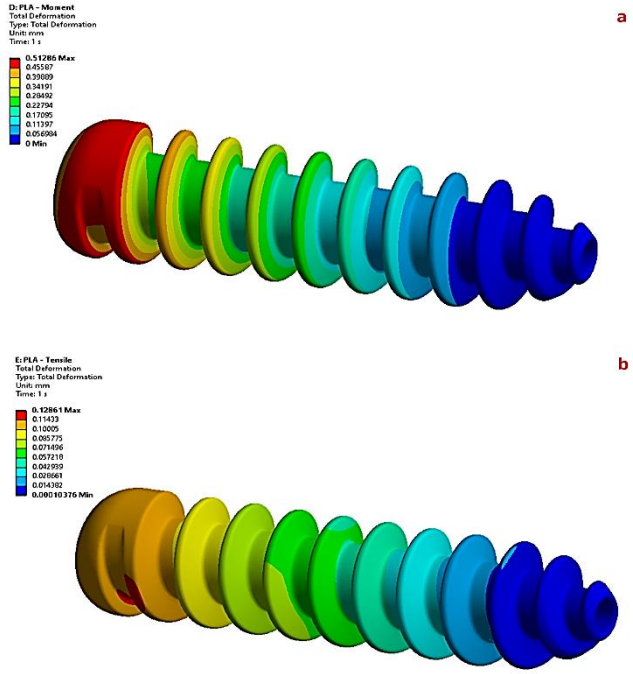

Fig. 8. Deformation under (a) torsional load (b) tensile load

4. Comparison

Table 3 presents the equivalent stresses and deformation results for titanium, PEEK, and PLLA. The results show that titanium exhibits the highest moment to failure and load to failure under torsional and tensile loads. PLLA exhibits the lowest results, and PEEK exhibits the intermediate results.

Table 3: Summary of results for titanium, PEEK, and PLA

	Moment Load			Tensile Load		
Material	Moment to Failure	Maximum Deformation	Maximum Equivalent Stress	Load to Failure	Maximum Deformation	Maximum Equivalent Stress
	Nm	mm	MPa	N	mm	MPa
Ti-6Al-4V	15.6027	0.318	1170	6493.1326	7.67E-02	1170
PEEK	1.542014841	0.90919	115	640.70989	0.20683	115
PLLA	0.797237093	0.51286	60	31.75958104	0.12861	60

Interference screws made of PEEK can withstand higher loads than PLLA, they may be less resistant to deformation than titanium. Results indicate that titanium screws have the maximum equivalent stress, implying greater load-bearing capacity, while PEEK and PLLA screws show lower equivalent stress values, suggesting they may not be as strong under heavy loads.

Notably, PLA interference screws demonstrate significantly less deformation under tensile loads compared to titanium and PEEK, indicating better resistance to bending or twisting. The choice of interference screw material depends on specific application requirements, including strength, durability, and deformation resistance. For applications prioritizing high strength and load-bearing capacity, titanium may be the preferred choice. Conversely, if resistance to deformation and bending is crucial, PLLA may offer a more suitable option.

5 Conclusion

Interference screws are widely used for the fixation of soft tissue-to-bone or bone-to-bone grafts. The selection of the appropriate material for interference screws is crucial. Different materials are used for these screws, including titanium, polyetheretherketone (PEEK), and poly-L-lactic acid (PLLA). This study compares the failure behavior and strength of various screws made of titanium, PLLA, and PEEK under tensile and torsion loads. Titanium alloy exhibits the highest strength, with a moment to failure of 15.60 Nm and a load to failure of 6493.13 N. Maximum equivalent stress is 1170 MPa for both load types. Deformation is minimal, at 0.318 mm under moment and 0.077 mm under tensile load, indicating high stiffness and durability. PEEK shows moderate strength with a moment to failure of 1.54 Nm and a load to failure of 640.71 N. Maximum equivalent stress is 115 MPa. Deformation is higher than titanium's, at 0.909 mm under moment and 0.207 mm under tensile load, reflecting its flexibility compared to metal's.

PLA has the lowest strength, with a moment to failure of 0.80 Nm and a load to failure of 31.76 N. Maximum equivalent stress is 60 MPa. Deformation is 0.513 mm under moment and 0.129 mm under tensile load, indicating that PLA is less suitable for high-load applications due to its lower strength and higher deformation. The minimum equivalent stress at the interference screw under torsional load occurs near the head and tail at the shortest diameter of the screw. While the maximum stress occurs at the largest diameter of the interference screw.

References

[1] A. M. Barrett, G. R. Barrett, and T. D. Brown, “Interference Screw Fixation in Bone–Patellar Tendon–Bone Anterior Cruciate Ligament Reconstruction,” The Anterior Cruciate Ligament: Reconstruction and Basic Science: Second Edition, pp. 322-326.e1, 2018.

[2] M. Hussain, S. M. Khan, M. Shafiq, N. Abbas, U. Sajjad, and K. Hamid, “Advances in biodegradable materials: Degradation mechanisms, mechanical properties, and biocompatibility for orthopedic applications,” Heliyon, vol. 10, no. 12, 2024.

[3] M. Hussain, S. M. Khan, K. Al-Khaled, M. Ayadi, N. Abbas, and W. Chammam, “Performance analysis of biodegradable materials for orthopedic applications,” Mater Today Commun, vol. 31, pp. 103167, 2022.

[4] M. Hussain, S. M. Khan, M. Shafiq, and N. Abbas, “A review on PLA-based biodegradable materials for biomedical applications,” Giant, vol. 18, pp. 100261, 2024.

[5] Y. H. Kim, M. Choi, and J. W. Kim, “Are titanium implants actually safe for magnetic resonance imaging examinations?”, Arch Plast Surg, vol. 46, no. 1, pp. 96, 2019.

[6] H. Ma, A. Suonan, J. Zhou, Q. Yuan, L. Liu, X. Zhao, X. Lou, C. Yang, D. Li, and Y. gang Zhang, “PEEK (Polyether-ether-ketone) and its composite materials in orthopedic implantation,” Arabian Journal of Chemistry, vol. 14, no. 3, pp. 102977, 2021.

[7] C. H. Fang, M. Li, Y. F. Zhang, and H. Liu, “Extra-articular migration of PEEK interference screw after anterior cruciate ligament reconstruction: a report of two cases,” BMC Musculoskelet Discord, vol. 22, no. 1, 2021.

[8] D. Xia, F. Yang, Y. Zheng, Y. Liu, and Y. Zhou, “Research status of biodegradable metals designed for oral and maxillofacial applications: A review,” Bioact Mater, vol. 6, no. 11, pp. 4186–4208, 2021.

[9] P. Hernigou and J. Pariat, “History of internal fixation with plates (part 2): new developments after World War II; compressing plates and locked plates,” Int Orthop, vol. 41, no. 7, pp. 1489–1500, 2017.

[10] L. Tian, N. Tang, T. Ngai, C. Wu, Y. Ruan, L. Huang, and L. Qin, “Hybrid fracture fixation systems developed for orthopaedic applications: A general review,” J Orthop Translat, vol. 16, pp. 1–13, 2019.

[11] C. Zhang, J. Lin, and H. Liu, “Magnesium-based Biodegradable Materials for Biomedical Applications,” in MRS Advances, Materials Research Society, pp. 2359–2364, 2018.

[12] R. Gorejová, L. Haverová, R. Oriňaková, A. Oriňak, and M. Oriňak, “Recent advancements in Fe-based biodegradable materials for bone repair,” Springer New York LLC., 2019.

[13] D. Bian, W. Zhou, J. Deng, Y. Liu, W. Li, X. Chu, P. Xiu, H. Cai, Y. Kou, B. Jiang, and Y. Zheng, “Development of magnesium-based biodegradable metals with dietary trace element germanium as orthopaedic implant applications,” Acta Biomater, vol. 64, pp. 421–436, 2017.

[14] D. Zhao, F. Witte, F. Lu, J. Wang, J. Li, and L. Qin, “Current status on clinical applications of magnesium-based orthopaedic implants: A review from clinical translational perspective,” Elsevier Ltd., 2017.

[15] X. Zhang, H. Zu, D. Zhao, K. Yang, S. Tian, X. Yu, F. Lu, B. Liu, X. Yu, B. Wang, W. Wang, S. Huang, Y. Wang, Z. Wang, and Z. Zhang, “Ion channel functional protein kinase TRPM7 regulates Mg ions to promote the osteoinduction of human osteoblast via PI3K pathway: In vitro simulation of the bone-repairing effect of Mg-based alloy implant,” Acta Biomater, vol. 63, pp. 369–382, 2017.

[16] Y. Zhang, J. Xu, Y. C. Ruan, M. K. Yu, M. O’Laughlin, H. Wise, D. Chen, L. Tian, D. Shi, J. Wang, S. Chen, J. Q. Feng, D. H. K. Chow, X. Xie, L. Zheng, L. Huang, S. Huang, K. Leung, N. Lu, L. Zhao, H. Li, D. Zhao, X. Guo, K. Chan, F. Witte, H. C. Chan, Y. Zheng, and L. Qin, “Implant-derived magnesium induces local neuronal production of CGRP to improve bone-fracture healing in rats,” Nat Med, vol. 22, no. 10, pp. 1160–1169, 2016.

[17] J. W. Lee, H. S. Han, K. J. Han, J. Park, H. Jeon, M. R. Ok, H. K. Seok, J. P. Ahn, K. E. Lee, D. H. Lee, S. J. Yang, S. Y. Cho, P. R. Cha, H. Kwon, T. H. Nam, J. H. Lo Han, H. J. Rho, K. S. Lee, Y. C. Kim, and D. Mantovani, “Long-term clinical study and multiscale analysis of in vivo biodegradation mechanism of Mg alloy,” Proc Natl Acad Sci U S A, vol. 113, no. 3, pp. 716–721, 2016.

[18] N. E. L. Saris, E. Mervaala, H. Karppanen, J. A. Khawaja, and A. Lewenstam, “Magnesium: An update on physiological, clinical and analytical aspects,” Clinica Chimica Acta, vol. 294, no. 1–2, pp. 1–26, 2000.

[19] J. Gonzalez, R. Q. Hou, E. P. S. Nidadavolu, R. Willumeit-Römer, and F. Feyerabend, “Magnesium degradation under physiological conditions – Best practice,” Bioact Mater, vol. 3, no. 2, pp. 174–185, 2018.

[20] M. Hussain, S. M. Khan, M. Shafiq, M. Al-Dossari, U. F. Alqsair, S. U. Khan, and M. I. Khan, "Comparative study of PLA composites reinforced with graphene nanoplatelets, graphene oxides, and carbon nanotubes: Mechanical and degradation evaluation," Energy, vol. 308, pp. 132917, 2024.

[21] M. Hussain, S. M. Khan, M. Shafiq, and N. Abbas, "Mechanical and Degradation Studies on the Biodegradable Composites of a Polylactic Acid Matrix Reinforced by Tricalcium Phosphate and ZnO Nanoparticles for Biomedical Applications," JOM, vol. 75, no. 12 pp. 5379–5387, 2023.

[22] S. W. On, S. W. Cho, S. H. Byun, and B. E. Yang, "Bioabsorbable Osteofixation Materials for Maxillofacial Bone Surgery: A Review on Polymers and Magnesium-Based Materials," Biomedicines, vol. 8 no. 9, 2020.

[23] Y. Matsuda, M. Karino, T. Okui, and T. Kanno, "Complications of Poly-l-Lactic Acid and Polyglycolic Acid (PLLA/PGA) Osteosynthesis Systems for Maxillofacial Surgery: A Retrospective Clinical Investigation," Polymers 2021, Vol. 13, Page 889, vol. 13, no. 6, pp. 889, 2021.

[24] T. M. B. K. dos Santos, C. Merlini, Á. Aragones, and M. C. Fredel, "Manufacturing and characterization of plates for fracture fixation of bone with biocomposites of poly (lactic acid-co-glycolic acid) (PLGA) with calcium phosphates bioceramics," Materials Science and Engineering: C, vol. 103, pp. 109728, 2019.

[25] M. E. Draenert, C. Martini, D. C. Watts, K. Draenert, and A. Wittig-Draenert, "Bone augmentation by replica-based bone formation," Dental Materials, vol. 36, no. 11, pp. 1388–1396, 2020.

[26] M. Bohner, B. L. G. Santoni, and N. Döbelin, "β-tricalcium phosphate for bone substitution: Synthesis and properties," Acta Biomater, vol. 113, pp. 23–41, 2020.

[27] M. D. Markel, "Bone Grafts and Bone Substitutes," Equine Fracture Repair, pp. 163–172, 2019.

[28] M. N. Collins, G. Ren, K. Young, S. Pina, R. L. Reis, and J. M. Oliveira, "Scaffold Fabrication Technologies and Structure/Function Properties in Bone Tissue Engineering," Adv Funct Mater, vol. 31, no. 21, pp. 2010609, 2021.

[29] I. R. Bordea, S. Candrea, G. T. Alexescu, S. Bran, M. Băciuț, G. Băciuț, O. Lucaciu, C. M. Dinu, and D. A. Todea, "Nano-hydroxyapatite use in dentistry: a systematic review," vol. 52, no. 2, pp. 319–332, 2020.

[30] M. L. Hasan, A. R. Padalhin, B. Kim, and B. T. Lee, "Preparation and evaluation of BCP-CSD-agarose composite microsphere for bone tissue engineering," J Biomed Mater Res B Appl Biomater, vol. 107, no. 7, pp. 2263–2272, 2019.

[31] Q. Nawaz, T. Fiedler, J. Biggemann, T. Fey, and A. R. Boccaccini, "Flexural strength of biopolymer coated bioactive glass (45S5) sintered struts for bone tissue engineering applications," Mater Lett, vol. 337, pp. 133957, 2023.